https://dx.doi.org/10.1016/j.fuel.2023.128195
This is the Pre-Published Version.

Mathematical Modeling of Puffing and Microexplosion in Emulsified Fuel Droplets Containing Several Bubbles: A Case Study on n-Dodecane/Water Droplet

Saroj Ray[a], Peng Zhang[b,*], Song Cheng[a,*]

[a] Department of Mechanical Engineering, The Hong Kong Polytechnic University, Hung Hom, Kowloon, Hong Kong

[b] Department of Mechanical Engineering, City University of Hong Kong, Kowloon Tong, Kowloon, Hong Kong

* Corresponding authors:

Peng Zhang, penzhang@cityu.edu.hk

Song Cheng, songryan.cheng@polyu.edu.hk

Abstract

This paper presents a theoretical model for microexplosion and puffing in a single isolated emulsion droplet at high ambient temperature and one atmospheric pressure. The model considered transient heating of the droplet, bubble growth dynamics, bubble motion, and bubble interactions (e.g., bubble coalescence). The bubble growth is determined by solving a modified Rayleigh equation which considered bubble interactions. The model considered multiple bubbles inside a fuel droplet which were not accounted for in the models proposed in previous studies. The model is applied to simulating the microexplosion of n-dodecane/water droplets. The simulated microexplosion delay times are compared with the experimental data from the literature, with good qualitative and quantitative agreements obtained. Results show that microexplosion delay time diminished by 40% and 50% for a 10-times increase in the initial bubble diameter and changing the bubble location from droplet center to 0.4 times the droplet radius, respectively. For multiple bubbles inside the droplet,

© 2023. This manuscript version is made available under the CC-BY-NC-ND 4.0 license https://creativecommons.org/licenses/by-nc-nd/4.0/

the microexplosion delay time converges to a minimum threshold value without further changing the bubble number. The simplified model bears practical potential in enabling spray combustion modeling of water-emulsified fuels with considerably reduced computational costs.

Keywords: microexplosion, bubble dynamics, bubble interactions, n-dodecane/water droplet, emulsified fuel, droplet heating

Nomenclature

a	acceleration (m/s^2)
Bi	Biot number
c_p	specific heat capacity at constant pressure (J/(kg K))
c_v	specific heat capacity at constant volume (J/(kg K))
CFD	computational fluid dynamics
D	diameter (m)
F	force (N) or integration constant
g	acceleration due to gravity (m/s^2)
h	heat transfer coefficient (W/(m^2 K))
IC	Internal Combustion
k	thermal conductivity (W/(m K))
L	Latent heat of vaporization (J/kg)
m	mass (kg)
MW	molecular weight
N	Total number of bubbles
NO_x	nitrogen oxides
ODE	ordinary differential equation
p	pressure (Pa s)
r	radial position (m)
R	radius (m)
Re	Reynolds number
R_g	gas constant (J/(kg K))

R_u universal gas constant (J/(K mol))

RMSE Root mean square error

t time (s)

t_c Heat diffusion timescale (s)

t_e Microexplosion delay time

T temperature (K)

u the radial component of velocity (m/s)

V terminal velocity (m/s) or volume

Greek letters

α thermal diffusivity (m^2/s)

β product of separation constant and droplet radius

γ surface tension (N/m)

λ separation constant

μ dynamic viscosity (Pa s)

υ kinematic viscosity (m^2/s)

ρ density (kg/m^3)

τ relaxation timescale (s)

Subscripts

1,2 The first bubble, the second bubble

atm atmospheric

b bubble

bp boiling point

d droplet

D drag

i ith bubble

l liquid

L large

n n^{th} root

S small

V viscous

0 initial

∞ ambient

1. Introduction

The use of emulsified fuel in spray combustion devices has been demonstrated with many benefits, including mitigating both particulate matter and NO_x (nitrogen oxides) emissions simultaneously [1]. One example is the implementation of water-in-diesel emulsion fuel in diesel engines, which can reduce NO_x emissions as the water lowers the adiabatic flame temperature and suppress particulate matter formation since fuel evaporation and fuel/air mixing is enhanced by microexplosion of fuel droplets [2, 3]. For highly viscous fuels such as biodiesel, bigger droplets are produced in IC (Internal Combustion) engines, and incomplete combustion can occur due to longer combustion time. The use of biodiesel-water emulsified fuels has been shown to overcome this issue by producing finer droplets due to microexplosions [4]. Several methods to lower IC engine emissions have been suggested and investigated such as the addition of nanoparticles, water, or alcohols with fuels [5, 6]. Implementing these methods also improved the performance of engines [7]. Due to the complex nature of processes involved in spray combustion, the effect of an individual parameter can be difficult to establish. To overcome these difficulties, several stochastic and deep-learning-based optimized models have been employed in recent studies [7, 8]. Another way to reduce these complexities is to focus on a simplified system (i.e., extract a part of these systems) and perform a detailed fundamental analysis. One particular example of the second approach is the studies of microexplosions in single isolated droplets, which have been investigated and found in application in IC engines fueled with emulsified fuels [9].

Microexplosion is the violent breakdown of multicomponent fuel droplets. On the other hand, puffing is the escape of vapor from the droplets without violent breakdown. The earliest study on microexplosion in burning two-component fuel droplets was carried out by Ivanov and Nefedov [10]. They found that adding water to fuel improves combustion due to

faster evaporation as a result of microexplosion. The rapid breakdown due to microexplosion leads to better mixing of fuel vapor with ambient gas [11]. Thus, microexplosion in emulsified fuel can cause secondary atomization and produce much finer droplets. This increases the surface-to-volume ratio and enhances the evaporation rate.

Several parameters such as ambient temperature, pressure, and the concentration of volatile components affect the occurrence of microexplosion. Microexplosion is observed above a critical value of temperature as nucleation is absent at low temperatures [12]. At temperatures where microexplosion occurs, it has been observed that microexplosion delay time (defined as the time taken for the onset of a breakdown of parent droplet into finer droplets) decreases with increasing ambient temperature [13]. Microexplosion also does not occur with too low or too high volatile component concentration [14]. When the concentration of the volatile component is high, droplet evaporation is fast and the droplet temperature becomes too low for nucleation [15]. When the concentration of the volatile component is low, the pressure build-up inside the nucleated bubbles is not strong enough to cause microexplosion [16].

Microexplosion in a multicomponent droplet has been studied experimentally by suspended droplet, falling droplet, and Leidenfrost techniques [17]. Wang et al. [18] elucidated that microexplosion depends on the stability of the droplet generation mode. They also concluded that the nucleation of the volatile component occurs at the droplet center vicinity of a falling droplet. Microexplosion in a droplet can trigger microexplosion of nearby droplets simultaneously [19]. Li et al. [20] corroborated that the level of droplet superheating affects the bubble formation inside droplets. Rao et al. [21] concluded that bubble growth can occur through the merging of two bubbles to form a bigger bubble. They also found that during droplets breakup, ligaments are formed and breakup can occur at the ligament tip or base to form secondary droplets [22]. Avulapati et al. [23] classified microexplosion into two

groups – strong and weak. A single nucleus (or vapor bubble) near the droplet center causes a strong microexplosion, while multiple nuclei result in a weak microexplosion and produce slightly coarser child droplets.

Modeling of microexplosion in droplets has also been attempted for many years, for instance, through computational fluid dynamics (CFD) models. A comprehensive CFD model for simulating microexplosion in droplets should include droplet heating, bubble nucleation, bubble growth, and droplet breakup. Table 1 reviews the various models proposed for microexplosion in droplets from the previous studies. In general, the CFD model developed in previous studies considers transient droplet heating, and the presence of one or two bubbles in the droplet, as well as bubble growth. These models are, however, computationally expensive to apply in practical spray combustion modeling where puffing/microexplosion of millions of droplets takes place simultaneously.

The high computational cost associated with CFD models can be greatly mitigated by using reasonably simplified analytical models with justified assumptions. A common approach used in analytical models for microexplosion in a droplet is solving the heat diffusion equation. Additionally, a criterion based on the boiling point of the volatile component is employed to find the microexplosion delay time. The reviewed analytical models (see Table 1) all considered droplet heating or interactions between droplets, whereas the presence of multiple bubbles in the droplet and their growth and interaction have been overlooked.

A theoretical model for microexplosion in a droplet is proposed in this study. The novelties of the proposed model are: (1) it considers multiple bubbles inside a droplet, and (2) bubble-to-bubble interactions are taken into account, which was neglected in the previous studies. Due to heterogeneous nucleation, many bubbles are formed inside droplets before the onset of microexplosion (see Fig. 1(c)). Therefore, motivated by experimental observations,

109 the present model includes multiple bubbles and their interactions. First, the formulation of a
110 single bubble in a droplet is rigorously developed and the results are thoroughly analyzed and
111 validated. Following this, the model is extended to handling multiple bubbles inside a droplet,
112 based on which, parameters affecting microexplosion characteristics are analyzed.

113 The remainder of this paper is organized as follows. The mathematical formulations,
114 including the governing equations and assumptions used in the model, are presented in
115 Section 2. The solution methodology implemented in the code for analyzing the
116 microexplosion of n-dodecane/water emulsion droplets is reported in section 3. This is
117 followed by validation of the model against experimental data from previous studies in
118 Section 4, where the effect of various parameters on microexplosion delay time was also
119 discussed. Finally, the important conclusions from this study are summarized in Section 5.

120

121 Table 1: Review of models for microexplosions in emulsified droplets.

Authors	Model descriptions	Remarks and findings
Law [11]	• A CFD model was developed • Included transient heat and mass diffusion inside the droplet	• Rapidly heating of multicomponent droplets can cause an onset of nucleation
Zeng and Lee [24]	• A numerical model was developed • Employed linear instability analysis to analyze the breakup of droplets • Considered a droplet with a bubble present at the droplet center	• The ratio of the child droplet diameter to the initial droplet diameter is relatively insensitive to the initial droplet diameter
Shinjo et al. [25]	• A comprehensive CFD model for microexplosion • The model considered a water sub-droplet inside the fuel droplet and a bubble inside the sub-droplet • Navier-Stokes equation, energy balance equations, and species balance equations were solved	• Fuel droplet breakup happened in a localized area • Droplet breakup is more violent for large water sub-droplet located near the droplet center
Guida et al. [26]	• A comprehensive CFD model was proposed • The effect of a bubble-to-droplet size ratio is investigated	• Bubble-to-droplet size ratio notably affects the droplet disintegration

Girin [27]	• Analyze the breakup of thin liquid fuel shells using linear stability analysis	• Predict the average size of child droplets produced after a violent breakup
Sazhin et al. [31]	• An analytical model based on the solution of a one-dimensional transient heat conduction equation in composite water-fuel emulsion droplets • Consider a spherical water sub-droplet at the center of the fuel droplet • Droplet evaporation is neglected	• Predict the microexplosion delay time reasonably well, except for smaller droplets with a diameter of less than 100 μm
Nissar et al. [33]	• Similar to Sazhin et al. [28] model • The model includes the droplet evaporation • Robin boundary condition was employed at the surface of the droplet	• For water/n-dododecane droplets, microexplosions occur well before the droplet surface temperature approaches the boiling point of n-dodecane
Antonov et al. [14]	• An analytical model based on the solution of the 1D heat equation • Bubble formation due to the boiling of volatile components is neglected	• The microexplosion delay time is significantly affected by the initial water sub-droplet location
Antonov et al. [30]	• Similar to Sazhin et al. [28] model Interaction between two or three closely placed droplets is included Bubble formation and their interaction are neglected	• Microexplosion first occurs on the leading droplet followed by the downstream droplet
Saha et al. [31]	• Numerical model of a droplet with flash boiling • Bubbles coalescence is neglected	• Microexplosion delay time decreases with increasing degree of superheat
Present study	• The theoretical model considered multiple bubbles in the droplet and their growth and interaction • Bubble-to-bubble interactions are considered	• Microexplosion delay time decreases with increasing bubble diameter • The microexplosion delay time is independent of the number of bubbles with a large number of bubbles

2. Theoretical considerations

The theoretical model considers a stationary liquid droplet with bubbles inside in a hot and quiescent ambient. The initial size of the bubbles is much smaller than that of the droplet. The droplet-bubble(s) system undergoes transient heating by hot ambient gas and can

expand radially. The bubble can move inside the droplet under the action of buoyancy and drag force. The schematic of the model for the case with one bubble is illustrated in Fig. 1.

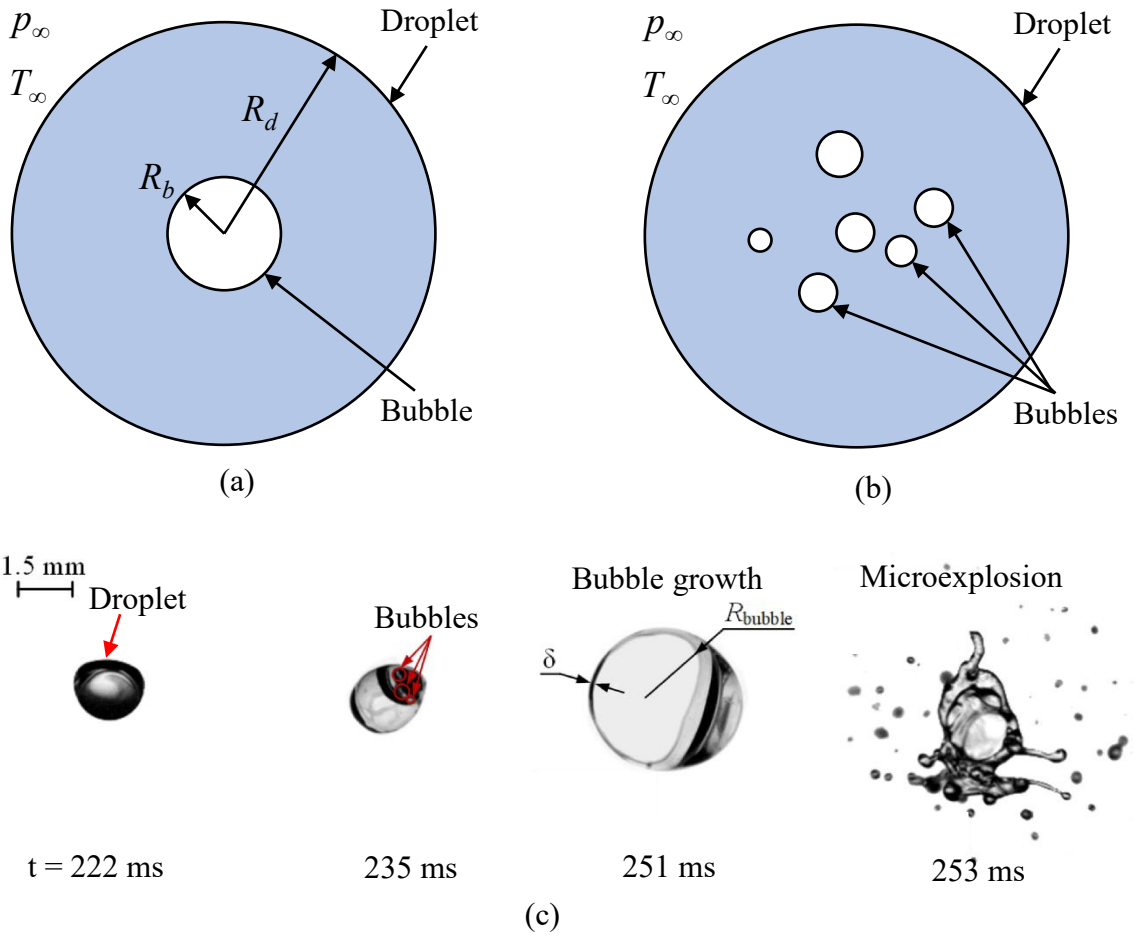

Figure 1. Schematic of (a) a bubble inside a droplet, (b) several bubbles inside a droplet, in a quiescent ambient at a temperature of T_∞ and pressure of p_∞, and (c) a series of images showing representative sequences of microexplosion in 90% rapeseed and 10% water droplet (T_∞ = 1223 K, D_{d0} = 1.680 mm) [14] (Reproduced from [14] with permission: License Number 5503490736683).

Several assumptions are made, including:

1) The droplet and bubbles are spherical throughout the analysis. This is justified as the droplet is stationary and the bubbles move with low velocity inside the droplet, thus, deformation is minor.
2) The liquid is assumed to be Newtonian.
3) Heat transfer from the ambient to the droplet is only through conduction and thus the Nusselt number is 2. The heat transfer from the droplet surface to the bubble is also through conduction as flow inside the droplet is neglected.
4) The temperature and pressure inside the bubble are uniform.
5) The bubble-droplet interface is in phase equilibrium and is governed by the Clausius-Clapeyron equation.
6) Evaporation at the droplet surface is neglected.
7) Bubbles coalesce spontaneously when they come in contact.
8) The physical properties are constant except for latent heat and bubble vapor density.

The liquid inside the droplet is Newtonian fluid (as per assumption 2), and the flow is radially outward (i.e., 1D) with constant liquid density. Thus, the conservation of mass inside the droplet is expressed as

$$\frac{\partial\left(r^2 u\right)}{\partial r} = 0, \tag{1}$$

where r is the radial position and u is the radial component of velocity inside the droplet, respectively. After integration in the liquid, Eq. (1) can be written as

$$r^2 u = R_b^2 \frac{dR_b}{dt} = F\left(t\right), \tag{2}$$

where R_b is the bubble radius at time t, and $F(t)$ is the constant of integration that can vary with time. Assumption 2 dictates the conservation of momentum in the liquid phase, and is given as,

$$\frac{\partial u}{\partial t}+u\frac{\partial u}{\partial r}=-\frac{1}{\rho_l}\frac{\partial p}{\partial r}+\nu_l\left[\frac{1}{r^2}\frac{\partial}{\partial r}\left(r^2\frac{\partial u}{\partial r}\right)-\frac{2u}{r^2}\right], \tag{3}$$

where p, ρ, and ν are the pressure, density, and kinematic viscosity, respectively, and subscript *l* indicates the liquid phase. An ordinary differential equation (ODE) for the bubble growth inside the droplet is obtained by integrating Eq. (3) for the liquid region using the two boundary conditions on the bubble-droplet interface and droplet surface (see Appendix, Eq. (A20)), and is given by

$$\frac{p_b-p_\infty}{\rho_l}=R_b\frac{d^2R_b}{dt^2}+\frac{3}{2}\left(\frac{dR_b}{dt}\right)^2+\frac{4\mu_l}{\rho_l R_b}\frac{dR_b}{dt}+\frac{2\gamma}{\rho_l R_b}+\frac{2\gamma}{\rho_l R_d}. \tag{4}$$

where p, R, μ, and γ are the pressure, radius, dynamic viscosity, and surface tension, respectively, and subscript *b*, *d* and ∞ denotes bubble, droplet, and ambient, respectively. Eq. (4) is a modified form of the Rayleigh equation [32] that captures the bubble growth with time, which was first derived for inviscid isothermal conditions by Rayleigh [33], then extended and applied to bubble expansion in superheated liquid by Plesset and Zwick [34] and Mikic et al. [35].

Droplet heating is governed by a one-dimensional transient heat equation in spherical coordinates following assumptions 2 and 3 and expressed as

$$\frac{\partial T}{\partial t}=\alpha\left(\frac{\partial^2 T}{\partial r^2}+\frac{2}{r}\frac{\partial T}{\partial r}\right), \tag{5}$$

where *T*, and α are the temperature and the thermal diffusivity, respectively. Assuming the velocity is small inside the droplet, the convection term is neglected in the above equation. The solution of Eq. (5) [36] is given by (see Appendix, Eq. (A.32))

$$T(r,t)=(T_0-T_\infty)\sum_{n=1}^{\infty}\frac{2(\sin\beta_n-\beta_n\cos\beta_n)}{(\beta_n-\sin\beta_n\cos\beta_n)}\frac{\sin(\beta_n\frac{r}{R_d})}{\beta_n\frac{r}{R_d}}e^{-\alpha\lambda_n^2 t}+T_\infty, \tag{6}$$

where T_0 is the initial droplet temperature, β_n is the n^{th} root of the transcendental equation $\tan(\beta_n) = \frac{\beta_n}{1-Bi}$, with $Bi = \frac{hR_d}{k}$, and λ_n is a separable constant, defined as $\lambda_n = \beta_n / R_d$. Since the droplet also contains bubbles, the properties of the liquid are modified and mixture properties are used (see Appendix, Eqs. (A34-A36)).

The motion of the bubble inside the droplet is also considered in the model. Due to buoyancy force, the bubble will move upward, and drag force acts on the bubble. Using Oseen's improvement to Stoke flow [37], the drag force is $6\pi\mu R_b \mathbf{v}\left(1+\frac{3}{16}Re\right)$, where Re is the Reynolds number and $\mathbf{v}$ is the bubble velocity. The force balance on the bubble is $F_V - F_D = ma$, where F_V, F_D, m, and a are the buoyancy force, drag force, bubble mass, and acceleration, respectively, which can be expressed as

$$\frac{4}{3}\pi R_b^3(\rho_l - \rho_b)g - 6\pi\mu R_b \mathbf{v}\left(1+\frac{3}{16}Re\right) = \frac{4}{3}\pi R_b^3 \rho_b a\,. \tag{7}$$

The analytical solution of Eq. (7) gives the location of the bubble and can be written as

$$x = V\tau e^{-t/\tau} + Vt + x_0 - V\tau\,, \tag{8}$$

and the velocity of the bubble is given by,

$$\mathbf{v} = -Ve^{-t/\tau} + V\,, \tag{9}$$

where $V = \frac{9\mu}{2R_b^2(\rho_l-\rho_b)g}\left(1+\frac{3}{16}\mathrm{Re}\right)$, $\tau = \frac{2R_b^2\rho_b}{9\mu\left(1+\frac{3}{16}\mathrm{Re}\right)}$, x_0, and g are the terminal velocity, relaxation timescale, initial bubble location, and acceleration due to gravity, respectively. In the case of multiple bubbles, bubbles coalescences are considered. For instance, from the mass balance of two coalescing bubbles,

$$\frac{p_{b1}R_{b1}^3}{T_{b1}}+\frac{p_{b2}R_{b2}^3}{T_{b2}}=\frac{p_bR_b^3}{T_b}. \tag{10}$$

The energy conservation for two coalescing bubbles can be written as

$$\left(4\pi R_{b1}^2\gamma+m_{b1}c_vT_{b1}\right)+\left(4\pi R_{b2}^2\gamma+m_{b2}c_vT_{b2}\right)=\left[4\pi R_b^2\gamma+\left(m_{b1}+m_{b2}\right)c_vT_b\right], \tag{11}$$

where c_v is the specific heat capacity of the water vapor, and subscripts 1 and 2 indicate the first and second coalescing bubbles. The pressure and radius of merged bubbles are found by solving Eqs. (10), and (11). The density of the bubble is calculated using the ideal gas law,

$$\rho_b=\frac{p_bV_b}{R_gT_b}, \tag{12}$$

where $R_g=\frac{R_u}{MW}$ is the gas constant, R_u is the universal gas constant and *MW* is the molecular weight. The vapor pressure inside the bubble is related to the temperature at the bubble-droplet interface by the Clausius-Clapeyron equation,

$$p_b=p_{atm}\exp\left[-\frac{L}{(R_u/MW)}\left(\frac{1}{T_b}-\frac{1}{T_{bp}}\right)\right], \tag{13}$$

where p_{atm}, T_{bp}, and L is the atmospheric pressure, the normal boiling point of water, and the latent heat of vaporization, respectively. Initially, the pressure inside the bubble is the equilibrium pressure.

3. Modeling n-dodecane/water droplets

The model developed in Section 2 is applied to modeling microexplosion in an n-dodecane/water droplet system. The reason for selecting the n-dodecane/water system is twofold: (i) it is a good representation of water-in-diesel emulsion fuels with wide applications that are already in place, and (ii) the availability of lab-scale experimental data

for model validation. To do so, Eqs. (4), (6), (8), (12), and (13) are solved to find R_b, T_b, x, p_b, and ρ_b, with specified initial and boundary conditions, and the respective fluid properties. Specifically, the initial droplet is assumed to consist of 15% water and 85% n-dodecane by volume with a uniform initial temperature of 300 K. The droplet is surrounded by ambient air with a uniform temperature that is higher than the initial droplet temperature. One (or multiple bubbles) with an initial diameter below 20% of the initial droplet diameter are placed at (or randomly distributed around) the center of the droplet at the start of the simulation. The bubble(s) is composed of 100% water vapor, with the same initial temperature as the droplet. The initial model parameters are summarized in Table 2. With the specified thermodynamic state from Table 2, the initial properties of the bubble are determined as those of water vapor, and the initial properties of the liquid phase in the droplet (i.e., a liquid mixture of water and n-dodecane) are determined following linear mixing rules, as shown in Table 3 for the case of 300 K initial temperature.

Table 2: Droplet, bubble, and gas properties.

Parameter	Value
Initial droplet diameter (D_{d0}) [μm]	50-175
Droplet initial composition (volume fraction)	0.15 water + 0.85 n-dodecane
Ambient gas composition	air
Bubble composition	water vapor
Initial bubble diameter (D_{b0})	0.02 D_{d0} - 0.2 D_{d0}
The initial number of bubbles	1-20
Initial droplet and bubble temperature [K]	300
Ambient temperature [K]	700-1073
Ambient pressure [atm]	1

Table 3. Thermo-physical properties [38] of liquid water, n-dodecane, and its mixture at 300 K.

Property	water	n-dodecane	0.15 water + 0.85 n-dodecane
Density [kg/m^3]	998	748	786

Thermal conductivity [W/(m K)]	0.60	0.14	0.23
Specific heat capacity at constant pressure [J/kg]	4184	2196	2575
Thermal diffusivity [m^2/s]	1.44×10^{-7}	8.52×10^{-8}	1.13×10^{-7}
Dynamic viscosity [mPa s]	1.00	1.35	1.29
Surface tension [mN/m]	72.8	25.4	49.2

Due to the higher ambient temperature than the droplet temperature, heat transfer will be initiated from the ambient toward the center of the droplet, and the bubble(s) will grow. As the bubble grows, the buoyance and drag forces become dynamic, and the bubble(s) will depart from the center of the droplet, whenever applicable. In the case of multiple bubbles, the bubbles are initially spaced randomly around the center from each other. Due to bubble dynamics (e.g., growing and floating), the bubbles might come into contact. Upon contact, the small bubbles coalesce into bigger bubbles with conservation in total mass and energy. The properties of the merged bubble are solved additionally using Eqs. (10) and (11). The model starts from time zero and terminates when any bubble-droplet interface reaches the droplet surface. The time from t=0 to the time of interface-surface contact is defined as the simulated microexplosion delay time (or puffing time). In this paper, time to puffing is assumed to be the same as microexplosion delay time (see more details in Section 4.2)

Since the explicit solutions for transient heat transfer are highly dependent on the solver timestep, a timestep dependency is carried out by varying the timestep from 0.1 μs to 100 μs. A timestep of 1 μs is selected and used in all analyses because it gives sufficiently accurate results with reasonable computational time. With this setting, it takes about 10 to 30 minutes (mostly depending on the number of bubbles considered) to perform each simulation on a 3.2 GHz kernel with 4 cores and 16 GB memory.

4. Results and discussion

4.1 Model validation

To validate the developed model, a droplet with a single bubble located at the droplet center is studied first, where normalized microexplosion delay times with various droplet diameters are computed and compared against the experimental data reported by Sazhin et al. [31]. The initial droplet diameter is varied from 50 μm to 175 μm with an increment of 25 μm, and the initial bubble diameter is fixed at 5 μm. The initial bubble diameter in the model is chosen implicitly, which is smaller than the initial droplet diameter by one order of magnitude. The microexplosion delay time at 50 μm is used to normalize the theoretical and experimental data. The ambient condition is set at 700 K and 1 atm, i.e., the same as the experimental conditions in [28].

The results are shown in Fig. 2, where microexplosion delay times are plotted against the initial droplet diameter. It is observed that the microexplosion delay time increases with an increase in initial droplet diameter. This is due to an increase in the droplet heat-up period, as it takes a long time to raise the droplet temperature by the same amount for a larger droplet as compared to a smaller droplet with the same droplet composition and temperature conditions. Also, the amount of energy available for bubble heating is less for bigger droplets, hence a slower bubble growth for larger droplets. The qualitative and quantitative comparison of the microexplosion delay time between the predicted results by the present model and the experimental data [28] is commendable. The root mean square error (RMSE) for normalized microexplosion delay time is 1.5%. The quantitative discrepancies could be due to neglecting droplet evaporation at the droplet surface, or the absence of convection motion inside the droplet.

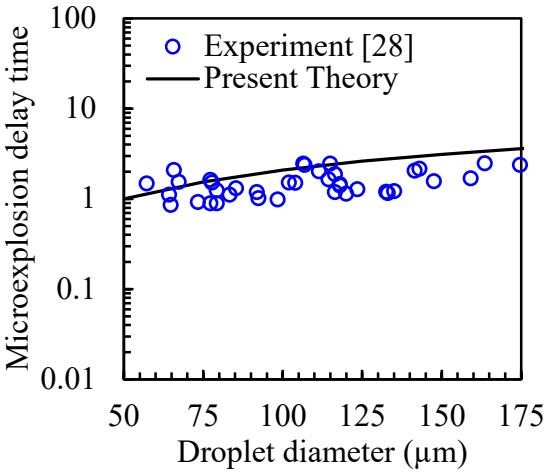

Figure 2. Comparisons of normalized microexplosion delay time predicted by the present theory (black solid line) against the experimental data (open circles) of Sazhin et al. [28] at various initial droplet diameters.

4.2 Parameters affecting microexplosion delay time

To get more insight into microexplosion characteristics, a parametric study is further carried out to understand the impact of various parameters, namely bubble diameter, bubble initial location, ambient temperature, and number of bubbles, on the microexplosion delay time. The parameter ranges varied are also summarized in Table 3.

Simulations are first performed to characterize bubble and droplet evolutions across different stages of microexplosion. Here, the initial droplet diameter is taken as 100 μm, which is representative of the average droplet size in spray combustion devices. An arbitrary small bubble located at the droplet center with an initial diameter of 0.05 times the droplet diameter is considered. The initial bubble diameter and location are fixed during modeling, except when the effect of bubble diameter and the number of bubbles is to be analyzed. For consistency and simplicity, the length and time are nondimensionalized with initial droplet diameter, D_{d0}, and heat diffusion time, $t_c = D_{d0}^2 / \alpha$, respectively, and the critical temperature of the water (647.3 K) and atmospheric pressure (1 atm) are used to

300 nondimensionalize the system temperatures and pressure, respectively. With these treatments,
301 the dimensionless temperature of the droplet, the bubble, and the ambient are 0.4634, 0.4634,
302 and 1.658, respectively, at the beginning.

303 Figure 3 shows the time evolution of the dimensionless bubble pressure (Fig. 3a),
304 bubble diameter (Fig. 3b), and droplet diameter (Fig. 3c) during microexplosion. It can be
305 first seen from Fig. 3a that the pressure inside the bubble increases nonlinearly with time. The
306 rise in the pressure is slow initially with time until 0.1, then relatively faster between the time
307 of 0.1 and 0.15, and much faster thereafter. These trends are explained as follows. At early
308 stages (e.g., time < 0.1), the droplet temperature is relatively low and the water evaporation
309 rate at the bubble-droplet interface is slow. As such, the amount of water vapor transferred
310 into the bubble from the bubble-droplet interface is small, and the pressure build-up inside
311 the bubble is relatively minor. As droplet heating continues and the droplet temperature rises
312 further (e.g., time > 0.1), the water evaporation rate becomes faster, and bubble pressure
313 increases more rapidly. The increased bubble pressure further expands the bubble-droplet
314 interface, leading to greater surface area at the interface that further enhances the water vapor
315 transfer rate into the bubble. This coupled effect eventually causes a sharp rise in the bubble
316 pressure at the latest stage (e.g., time > 0.15). During the transient heating process, the bubble
317 also moves upward due to buoyancy force. At the dimensionless time of 0.162, the bubble
318 surface makes contact with the droplet surface and puffing occurs.

319 For microexplosion to occur, the bubble pressure value must exceed a certain critical
320 value. Further experimental evidence is required to determine the critical pressure value for
321 violent disintegration, which is not available so far, as well as beyond the scope of this study.
322 Since the pressure rise is rapid during the latest stage, it is hypothesized here that the
323 microexplosion takes place at a moment very close to puffing. This justifies coinciding
324 microexplosion delay time and time to puffing in this study.

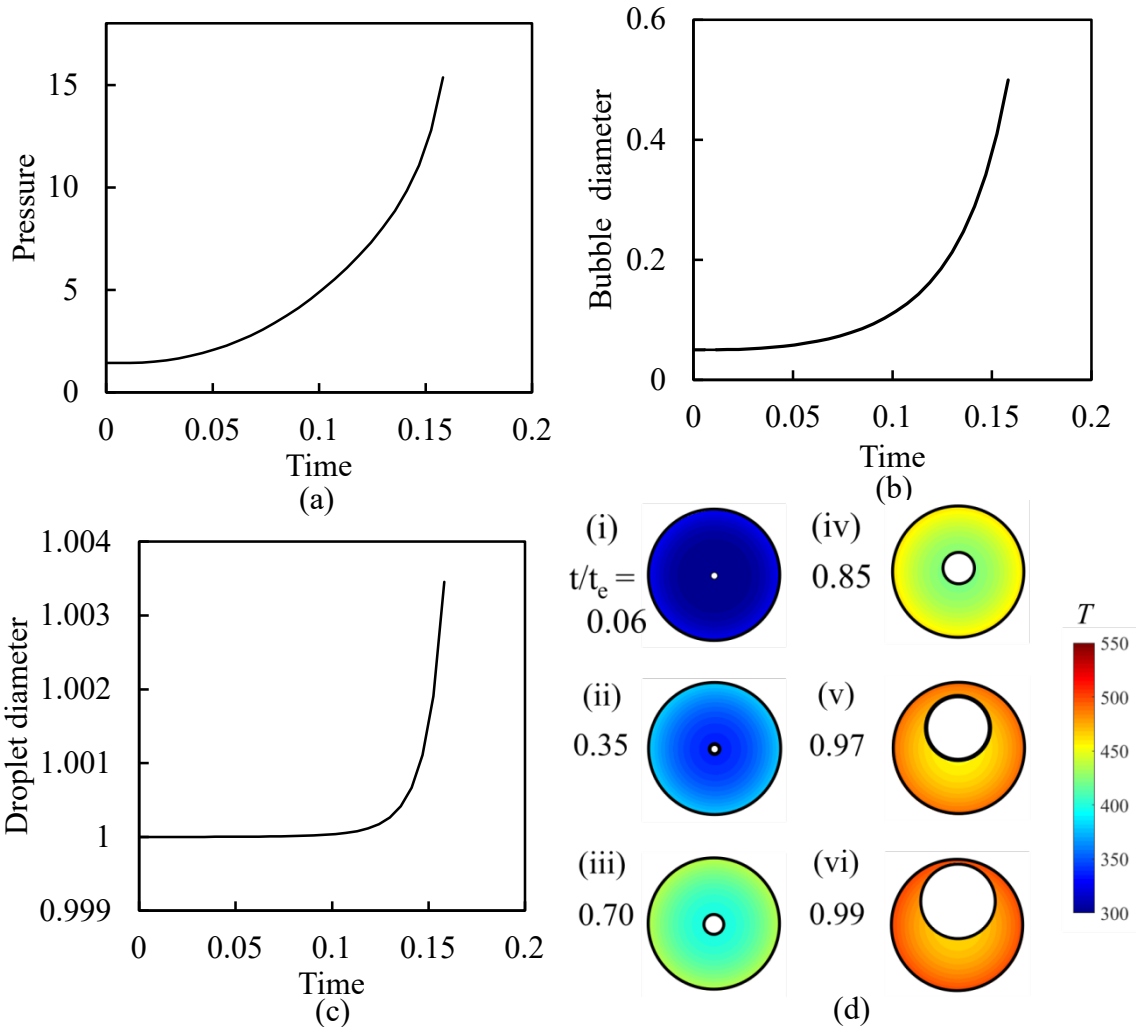

Figure 3. Variation in dimensionless (a) bubble pressure, (b) bubble diameter, and (c) droplet diameter with dimensionless time as predicted by the present theory. (d) shows the bubble expansion and temperature contour inside the droplet at several time instances.

The temporal evolutions of dimensionless bubble diameter and droplet diameter are shown in Figs. 3b and 3c, respectively, which follow similar qualitative trends to those observed in Fig. 3a, indicating the positive correlation between these parameters and their consistent impact on microexplosion characteristics. Despite the similar qualitative trends, differences are also observed between these parameters. This is the most obvious when comparing Fig. 3a with Fig. 3c, where the droplet diameter does not change noticeably until

337 the dimensionless time of 0.11, whereas this threshold is reached much earlier for the
338 dimensionless pressure profile. This is somewhat expected since the expansion of the droplet
339 is mainly contributed by the expansion of the bubble inside. In the early stages, since the
340 initial bubble size is considerably smaller than the droplet and the bubble growth rate is low,
341 the change in bubble volume per unit of time does not result in a significant change in the
342 droplet volume. In contrast, at later stages, the bubble growth rate amplifies and the bubble-
343 droplet interface rapidly approaches the droplet surface, thus pushing the droplet to grow
344 faster in size. This is evident from Fig. 3(d) that the bubble size does not change much in the
345 early stage while it expands rapidly in the later stage. Just before the onset of microexplosion,
346 the bubble diameter increased by 900% whereas the droplet diameter only grows by 0.34%.
347 The void fraction at this instant is 0.20 which is lower than the critical void fraction value of
348 0.55 used by Kawano et al. [39]. This difference in the void fraction (defined as the ratio of
349 bubble volume to the sum of bubble and droplet volumes) still can cause a small change in
350 microexplosion delay time due to the rapid expansion of the bubble in the later stage.

351 Figure 4 shows the variation in dimensionless microexplosion delay time with the
352 initial bubble diameter varying from 2% to 20% of the initial droplet diameter (i.e., 100 μm).
353 First seen is the strong and somewhat nonlinearly dependence of microexplosion delay time
354 on initial bubble diameter, where the microexplosion delay time decreases monotonically
355 with increasing initial bubble diameter. Increasing the bubble diameter by 10 times (i.e. one
356 order of magnitude change) results in a reduction of microexplosion delay time by 40%. This
357 can be attributed to (i) the greater buoyancy force applied on bubbles with larger initial
358 diameter, which enables a faster upward motion of the bubble to make it reach the droplet
359 surface earlier; and (ii) the greater surface area associated with larger bubbles, which
360 enhances water vapor transfer into the bubble, hence faster bubble growth.

The single-bubble-single-droplet model developed in this study assumes that the bubble is located at the center of the droplet, whereas in reality, the bubbles that form during nucleation may not. Therefore, it is important to analyze the effect of bubble formation at offset positions on the microexplosion delay time. To this end, the dimensionless bubble location is varied from 0 to 0.4 (with 0 and 0.4 indicating that the bubble center is initially at the droplet center and 40% droplet diameter above the droplet center, respectively), while the bubble and droplet diameters are kept the same. Note that the bubble center location was adjusted only vertically along the radial direction. Figure 5 summarizes the calculated dimensionless microexplosion delay time with different initial bubble positions. It is seen that the dimensionless microexplosion delay time decreases monotonically as the bubble deviates from the droplet center, by nearly 50% when the initial bubble location moves from 0 to 0.4. When the bubble is located near the droplet surface, the thermal resistance from the droplet surface to the bubble-droplet interface becomes smaller (i.e., reduced thickness of liquid phase between ambient and bubble-droplet interface), which leads to a higher heat transfer rate to the bubble, hence more rapid bubble pressure rise and faster bubble growth. In addition, the bubble only needs to travel a shorter distance (both upward by buoyancy and horizontally by bubble growth) to come in contact with the droplet surface for puffing to occur. Both these effects reduce the microexplosion delay time, as observed in Fig. 5.

To analyze the effect of ambient temperature on microexplosion delay time, the dimensionless ambient temperature is varied from 1.25 to 2.00. The predicted microexplosion delay times are illustrated in Fig. 6. The results indicate that microexplosion delay time decreases linearly with dimensionless temperature, due primarily to the increased heat transfer rate with higher ambient temperature. This trend agrees qualitatively with the experimental data reported by Antonov et al. [14], where water-diesel blends were used.

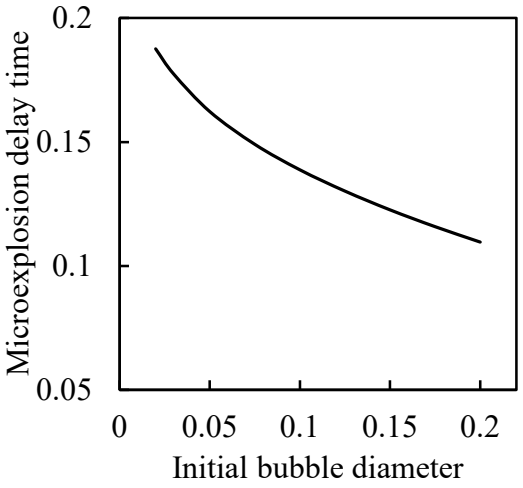

386

387

388 Figure 4. Variation in dimensionless microexplosion delay time with dimensionless initial

389 bubble diameter.

390

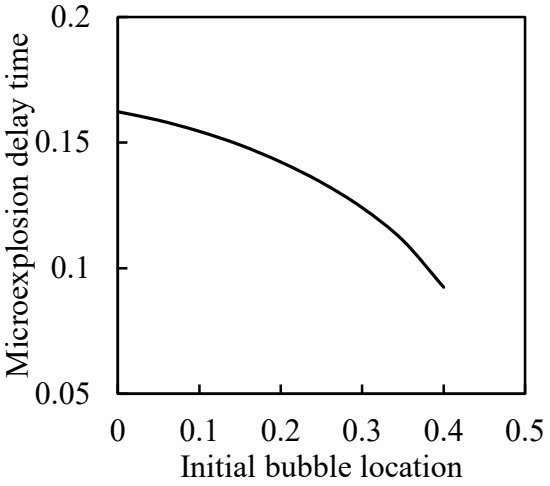

391

392 Figure 5. Variation in dimensionless microexplosion delay time with the dimensionless initial

393 bubble location.

394

395 Interactions of two unequal-size bubbles in droplets are shown in Fig. 7. It

396 shows four different time instants corresponding near the beginning, before bubbles

397 coalescence, after bubbles coalescence, and near the onset of microexplosion (marked as A, B,

398 C, and D stages), respectively. In Fig. 7(a), the bottom bubble is the big bubble, which

399 experiences buoyancy force and moves upward, and subsequently merged with the small
400 bubble. In the case of the big bubble above the small bubble as shown in Fig. 7(b), the big
401 bubble moves upward and the gap between bubbles can increase first. Then, after sufficient
402 heating of the small bubble, it can expand and move toward the big bubble and coalesce.
403 Thus, it takes a longer time for bubbles to coalesce in the second case.
404

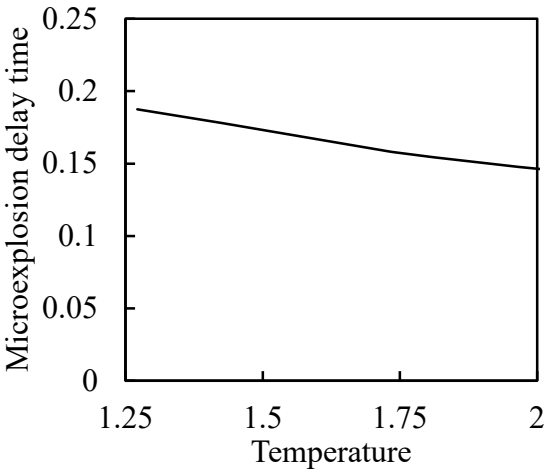

405

406 Figure 6. Variation of the dimensionless microexplosion delay time with dimensionless
407 ambient temperature.
408

409 In general, multiple bubbles can form at heterogeneous sites inside a droplet during
410 nucleation. Under such scenarios, the impact of microexplosion due to the presence of
411 multiple bubbles should be analyzed. This is achieved in the developed model by placing
412 multiple bubbles randomly inside the droplet. It is assumed that all the bubbles have the same
413 initial diameter (5 μm) and initially none of them touch each other. The initial location of
414 these bubbles is restrained to one-fourth of the droplet diameter to ensure the bubbles are
415 present near the droplet core.
416

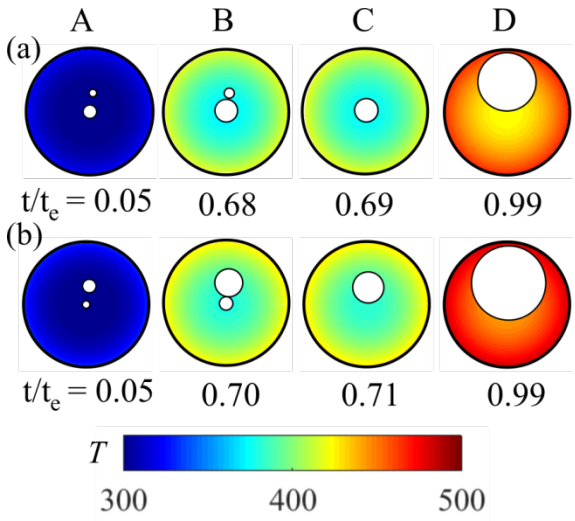

Figure 7. Interaction of two unequal-size bubbles inside a droplet. (a) the small bubble above the big bubble, and (b) the big bubble above the small bubble. (T_∞ = 1073.15 K, R_{d0} = 100 µm, $R_{b0,S}$ = 2.5 µm, $R_{b0,L}$ = 5.0 µm)

The predicted microexplosion delay times with the number of bubbles changing from 1 to 20 are shown in Fig. 8. A sharp decrease in microexplosion delay time is observed as the number of bubbles increases from 1 to 10, while the decreasing trend diminishes gradually when the number of bubbles further increases from 10 to 20. Eventually, the predicted microexplosion delay time converges to a minimum threshold value without further changing with the bubble number. During the transient heating of a multi-bubble droplet, each bubble can expand and move inside the droplet. These bubbles will first undergo bubble growth and then merges into a bigger bubble upon contact. When there are only a few bubbles in the droplet (e.g., bubble number < 5 in Fig. 8), each bubble has more space for self-growth, hence a longer residence time for the individual bubbles before bubble coalescence. In such situations, microexplosion is governed by both the dynamics of individual bubbles and the dynamics of the coalesced bubble. As adding more bubbles into the droplet will increase the initial surface area for mass transfer of water vapor and heat transfer into the individual bubbles, individual bubble growth will be facilitated and microexplosion delay time is

436 expected to decrease (as discussed with Figs. 3 and 4). However, when the droplet is over-
437 populated with bubbles (e.g., bubble number > 15 in Fig. 8), the initial bubbles will quickly
438 coalesce without significant individual bubble growth. In such a case, microexplosion is
439 dominated primarily by the dynamics of the coalesced bubble and becomes insensitive to the
440 number of initial bubbles. It should be noted that the converged microexplosion delay time is
441 independent of the location of the initial bubbles, though they are randomly generated during
442 the simulation. This result is one of the important findings of this study. The location of the
443 initial bubbles will only affect the prediction results when individual bubble growth is
444 impactful (e.g., bubble number < 15 in Fig. 8).
445

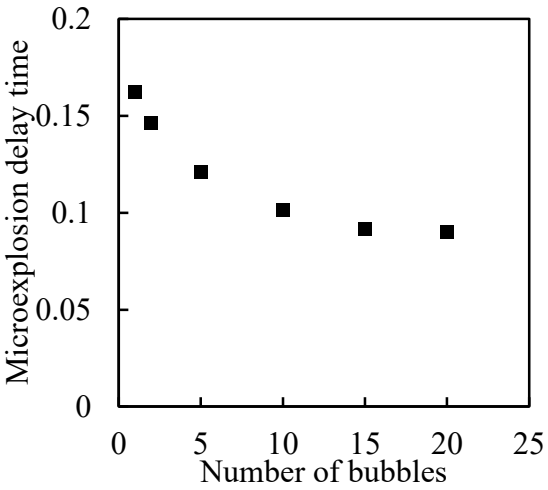

446
447 Figure 8. Variation in dimensionless microexplosion delay time with the different number of
448 bubbles.
449
450 **5. Conclusions and prospects**
451 This paper proposes a theoretical model for microexplosion and puffing in a droplet
452 that accounts for nucleation, bubble dynamics (e.g., growth and buoyancy), and bubble-to-
453 bubble interactions (e.g., coalescence), which is developed based on conservation laws of

mass, momentum, and energy under frameworks of one-dimensional transient heat transfer across the droplet and phase equilibrium at the bubble-droplet interface.

The model is immediately demonstrated with a case study of an n-dodecane/water droplet in hot air, where microexplosion is modeled for a single-bubble droplet system with various initial droplet diameters. Microexplosion delay times are then characterized from the simulation results and compared against literature experiments, with a reasonable quantitative agreement and commendable qualitative agreement obtained.

Given the commendable performance of the model, it is further employed to characterize bubble and droplet evolutions during microexplosion, via changes in three dimensionless quantities, namely bubble pressure, bubble diameter, and droplet diameter. Two characteristically different stages of microexplosion are observed for all three quantities, where they exhibit minor-to-moderate and drastic evolutions at early and later stages of microexplosion, respectively.

Thereafter, the effect of initial bubble diameter, location, and number are analyzed, where it is found that microexplosion characteristics are strongly linked to bubble dynamics, bubble-to-bubble interactions, as well as the associated heat diffusion process. Microexplosion delay time decreases by 40% with the 10-times increase in the bubble diameter, whereas it drops by 50% when the initial bubble location moves from 0 (i.e., at droplet center) to 0.4 (near the droplet surface). Higher ambient temperatures diminish microexplosion delay time. It is interesting to note that the predicted microexplosion delay time eventually converges to a minimum threshold value regardless of a further increase in the number of initial bubbles, implying a saturated promoting effect of fuel emulsification on microexplosion. Microexplosion delay time declines by 50% when the number of bubbles increases from 1 to 15, whereas it only diminishes by 3% for further increasing the number of bubbles to 20. The main limitations of the present model are that the evaporation at the

droplet surface is neglected and the assumption of constant properties, which will be relaxed in a forthcoming study. The developed model offers a potential for modeling practical spray combustion with significantly mitigated computational effort and sufficient fidelity.

Most of the theoretical and numerical models reported in previous studies, including the model used in the present study, neglect combustion in the gas phase. Models for microexplosion in emulsified droplets with combustion can be developed in the future. These models have applications in diesel engines running on emulsified fuel such as biodiesel blended with water or alcohol.

Acknowledgments

The work described in this paper was supported by grants from the Research Grants Council of the Hong Kong Special Administrative Region, China (Nos. CityU 15222421, CityU 15218820, PolyU P0034937, and PolyU P0039589).

References

[1] I. Glassman, R. A. Yetter, N. G. Glumac, Combustion, Academic Press, 2015.

[2] A. M. Attia, A. R. Kulchitskiy, Influence of the structure of water-in-fuel emulsion on diesel engine performance, Fuel 116 (2014) 703-708. https://doi.org/10.1016/j.fuel.2013.08.057

[3] O. A. Elsanusi, M. M. Roy, M. S. Sidhu, Experimental investigation on a diesel engine fueled by diesel-biodiesel blends and their emulsions at various engine operating conditions, Applied Energy 203 (2017) 582-593. https://doi.org/10.1016/j.apenergy.2017.06.052

503 [4] M. S. R. Dandu, K. Nanthagopal, B. Ashok, D. Balasubramanian, and R. Sakthivel,
504 Impact of NOx control measures on engine life. NOx Emission Control Technologies in
505 Stationary and Automotive Internal Combustion Engines, (2022) 387-421.
506 https://doi.org/10.1016/B978-0-12-823955-1.00013-9
507 [5] H. Fayaz, M. A. Mujtaba, M. E. M. Soudagar, L. Razzaq, S. Nawaz, M. A. Nawaz, M.
508 Farooq, A. Afzal, W. Ahmed, T. Y. Khan, S. Bashir, H. Yaqoob, A. I. EL-Seesy, S. Wageh,
509 A. Al-Ghamdi, and A. Elfasakhany, Collective effect of ternary nano fuel blends on the
510 diesel engine performance and emissions characteristics. Fuel 293 (2021) 120420.
511 https://doi.org/10.1016/j.fuel.2021.120420
512 [6] A. M. Ithnin, W. J. Yahya, M. A. Ahmad, N. A. Ramlan, H. A. Kadir, N. A. C. Sidik, T.
513 Koga, Emulsifier-free Water-in-Diesel emulsion fuel: Its stability behaviour, engine
514 performance and exhaust emission, Fuel 215 (2018) 454-462.
515 https://doi.org/10.1016/j.fuel.2017.11.061
516 [7] O. D. Samuel, M. A. Waheed, A. Taheri-Garavand, T. N. Verma, O. U. Dairo, B. O.
517 Bolaji, and A. Afzal, Prandtl number of optimum biodiesel from food industrial waste oil and
518 diesel fuel blend for diesel engine. Fuel 285 (2021) 119049.
519 https://doi.org/10.1016/j.fuel.2020.119049
520 [8] P. Atarod, E. Khlaife, M. Aghbashlo, M. Tabatabaei, A. T. Hoang, H. Mobli, M. H.
521 Nadian , H. Hosseinzadeh-Bandbafha. P. Mohammadi, T. R. Shojaei, and O. Mahian, Soft
522 computing-based modeling and emission control/reduction of a diesel engine fueled with
523 carbon nanoparticle-dosed water/diesel emulsion fuel. Journal of Hazardous Materials 407
524 (2021) 124369. https://doi.org/10.1016/j.jhazmat.2020.124369
525 [9] D. V. Antonov, R. M. Fedorenko, and P. A. Strizhak, Micro-Explosion Phenomenon:
526 Conditions and Benefits. *Energies 15*(20) (2022) 7670. https://doi.org/10.3390/en15207670

527 [10] V. M. Ivanov, P. I. Nefedov, Experimental investigation of the combustion process of
528 natural and emulsified liquid fuels, NASA TT F-258 (1965) 1-23.
529 [11] C. K. Law, Internal boiling and superheating in vaporizing multicomponent
530 droplets, AIChE Journal 24(4) (1978) 626-632. https://doi.org/10.1002/aic.690240410
531 [12] D. V. Antonov, R. S. Volkov, P. A. Strizhak, An explosive disintegration of heated fuel
532 droplets with adding water, Chemical Engineering Research and Design 140 (2018) 292-307.
533 https://doi.org/10.1016/j.cherd.2018.10.031
534 [13] D. V. Antonov, G. V. Kuznetsov, S. Y. Misyura, P. A. Strizhak, Temperature and
535 convection velocities in two-component liquid droplet until micro-explosion, Experimental
536 Thermal and Fluid Science 109 (2019) 109862.
537 https://doi.org/10.1016/j.expthermflusci.2019.109862
538 [14] D. V. Antonov, R. M. Fedorenko, G. V. Kuznetsov, P. A. Strizhak, Modeling the micro-
539 explosion of miscible and immiscible liquid droplets, Acta Astronautica 171 (2020) 69-82.
540 https://doi.org/10.1016/j.actaastro.2020.02.040
541 [15] W. B. Fu, L. Y. Hou, L. Wang, F. H. Ma, A unified model for the micro-explosion of
542 emulsified droplets of oil and water, Fuel Processing Technology 79(2) (2002) 107-119.
543 https://doi.org/10.1016/S0378-3820(02)00106-6
544 [16] H. Watanabe, Y. Suzuki, T. Harada, Y. Matsushita, H. Aoki, T. Miura, An experimental
545 investigation of the breakup characteristics of secondary atomization of emulsified fuel
546 droplet, Energy 35(2) (2010) 806-813. https://doi.org/10.1016/j.energy.2009.08.021
547 [17] E. Mura, R. Calabria, V. Califano, P. Massoli, J. Bellettre, Emulsion droplet micro-
548 explosion: Analysis of two experimental approaches, Experimental Thermal and Fluid
549 Science 56 (2014) 69-74. https://doi.org/10.1016/j.expthermflusci.2013.11.020

[18] C. H. Wang, X. Q. Liu, C. K. Law, Combustion and microexplosion of freely falling multicomponent droplets, Combustion and flame 56(2) (1984) 175-197. https://doi.org/10.1016/0010-2180(84)90036-1

[19] H. Z. Sheng, L. Chen, C. K. Wu, The droplet group micro-explosions in W/O diesel fuel emulsion sprays, SAE transactions (1995) 1534-1542. https://www.jstor.org/stable/44633318

[20] S. Li, Y. Zhang, W. Qi, and B. Xu, Quantitative observation on characteristics and breakup of single superheated droplet, *Experimental Thermal and Fluid Science*, *80* (2017) 305-312. https://doi.org/10.1016/j.expthermflusci.2016.09.004

[21] D. C. K. Rao, S. Karmakar, and S. Basu, Atomization characteristics and instabilities in the combustion of multi-component fuel droplets with high volatility differential, *Scientific reports*, *7*(1) (2017) 1-15 https://doi.org/10.1038/s41598-017-09663-7

[22] D. C. K. Rao, S. Karmakar, and S. Basu, Bubble dynamics and atomization mechanisms in burning multi-component droplets, *Physics of Fluids*, *30*(6) (2018) 067101. https://doi.org/10.1063/1.5035384

[23] M. M. Avulapati, T. Megaritis, J. Xia, L. Ganippa, Experimental understanding on the dynamics of micro-explosion and puffing in ternary emulsion droplets, Fuel 239 (2019) 1284-1292. https://doi.org/10.1016/j.fuel.2018.11.112

[24] Y. Zeng, C. F. Lee, Modeling droplet breakup processes under micro-explosion conditions, Proceedings of the Combustion Institute 31(2) (2007) 2185-2193. https://doi.org/10.1016/j.proci.2006.07.237

[25] J. Shinjo, J. Xia, L. C. Ganippa, A. Megaritis, Physics of puffing and microexplosion of emulsion fuel droplets, Physics of Fluids 26(10) (2014) 103302. https://doi.org/10.1063/1.4897918

573 [26] P. Guida, A. Ceschin, F. E. H. Pérez, H. G. Im, W. L. Roberts, Computationally-derived
574 submodel for thermally-induced secondary atomization, International Journal of Heat and
575 Mass Transfer 199 (2022) 123448. https://doi.org/10.1016/j.ijheatmasstransfer.2022.123448
576 [27] O. G. Girin, Dynamics of the emulsified fuel drop microexplosion, Atomization and
577 Sprays 27(5) (2017) 407-422. https://doi.org/10.1615/AtomizSpr.2017017143
578 [28] S. S. Sazhin, O. Rybdylova, C. Crua, M. Heikal, M. A. Ismael, Z. Nissar, A. R. B. Aziz,
579 A simple model for puffing/micro-explosions in water-fuel emulsion droplets, International
580 Journal of Heat and Mass Transfer 131 (2019) 815-821.
581 https://doi.org/10.1016/j.ijheatmasstransfer.2018.11.065
582 [29] Z. Nissar, O. Rybdylova, S. S. Sazhin, M Heikal, A. R. B. Aziz, M. A. Ismael, A model
583 for puffing/microexplosions in water/fuel emulsion droplets, International Journal of Heat
584 and Mass Transfer 149 (2020) 119208.
585 https://doi.org/10.1016/j.ijheatmasstransfer.2019.119208
586 [30] D. V. Antonov, R. M. Fedorenko, P. A. Strizhak, G. Castanet, S. S. Sazhin,
587 Puffing/micro-explosion of two closely spaced composite droplets in tandem: Experimental
588 results and modelling, International Journal of Heat and Mass Transfer 176 (2021) 121449.
589 https://doi.org/10.1016/j.ijheatmasstransfer.2021.121449
590 [31] A. Saha, T. Grenga, A. Y. Deshmukh, J. Hinrichs, M. Bode, and H. Pitsch, Numerical
591 modeling of single droplet flash boiling behavior of e-fuels considering internal and external
592 vaporization. Fuel 308 (2022) 121934. https://doi.org/10.1016/j.fuel.2021.121934
593 [32] S. S. Sazhin, Processes in Composite Droplets. In Droplets and Sprays: Simple Models
594 of Complex Processes, Springer, Cham 2022, 277-325.
595 [33] L. Rayleigh, On the pressure developed in a liquid during the collapse of a spherical
596 cavity, The London, Edinburgh, and Dublin Philosophical Magazine and Journal of Science
597 34 (1917) 94 – 98. https://doi.org/10.1080/14786440808635681

598 [34] M. S. Plesset, S. A. Zwick, The growth of vapor bubbles in superheated liquids, Journal
599 of applied physics 25(4) (1954) 493-500. https://doi.org/10.1063/1.1721668
600 [35] B. B. Mikic, W. M. Rohsenow, P. Griffith, On bubble growth rates, International Journal
601 of Heat and Mass Transfer 13(4) (1970) 657-666. https://doi.org/10.1016/0017-
602 9310(70)90040-2
603 [36] D. W. Hahn, M. N. Ozisik, Heat Conduction, third ed., John Wiley & Sons, 2012.
604 [37] G. K. Batchelor, An introduction to fluid dynamics, Cambridge university press, 2000.
605 [38] R. C. Reid, J. M. Prausnitz, B. E. Poling, The properties of gases and liquids, fourth
606 ed., McGraw-Hill Inc., New York, 1987.
607 [39] D. Kawano, Y. Goto, M. Odaka, and J. Senda, Modeling atomization and vaporization
608 processes of flash-boiling spray. SAE Technical Paper (2004),
609 doi:https://doi.org/10.4271/2004-01-0534.